Plume reduction in segmented electrode Hall thruster

Y. Raitses,[a] L. A. Dorf, A. A. Litvak, and N. J. Fisch

Princeton Plasma Physics Laboratory, Princeton University, Princeton, New Jersey 08543

A segmented electrode, which is placed at the thruster exit, is shown to affect thruster operation in several ways, whether the electrode produces low emission current or no emission current, although there appear to be advantages to the more emissive segmented electrode. Measured by plume divergence, the performance of Hall thruster operation, even with only one power supply, can approach or surpass that of nonsegmented operation over a range of parameter regimes. In particular, the low gas flow rate can exhibit low plume divergence. This allows flexibility in operation of segmented electrode thrusters in variable thrust regimes. © *2000 American Institute of Physics.* [S0021-8979(00)02615-3]

I. INTRODUCTION

The main advantage of using electric propulsion for space-craft orbit control is the larger jet velocity (10–100 km/s), which enables significant savings in the propellant mass. Chemical rockets are limited to exhaust speeds of about 3 km/s. The Hall thruster is particularly suited for many space applications that are limited either in time or in fuel mass. The principle of Hall thruster operation is based on the electrostatic acceleration of ions in crossed electric and magnetic fields applied in a quasineutral plasma of a dc electric discharge.[1] Hall thrusters are typically coaxial (see Fig. 1), consisting of a magnetic circuit, anode (which can also be a gas distributor), ceramic channel, and cathode neutralizer. A gas propellant, typically xenon, enters the channel through the anode and is ionized by impact with energetic electrons of the electrical discharge. The applied radial magnetic field impedes the axial electron motion towards the anode. The impeded electrons can then more effectively ionize the propellant atoms and support a significant axial electric field with equipotentials along the magnetic-field lines ($E = -v_e \times B$). The axial field accelerates the ions towards the channel exhaust, where they are neutralized by electrons from the cathode neutralizer. The thrust is a reaction force to this electrostatic acceleration, applied to the magnetic circuit.

Existing Hall thrusters can efficiently produce large jet velocities of 10–20 km/s with input power in the range from several hundred watts to a few tens of kilowatts.[2] Since ion acceleration takes place in a quasineutral plasma, these thrusters are not limited by space-charge buildup. Hence, higher current and thrust densities than conventional electrostatic ion thrusters can be achieved at discharge voltages of hundreds of volts. Hall thrusters are also gridless, a feature that is useful for certain industrial applications of plasma sources.

The key drawback of Hall thrusters as compared to ion thrusters is large beam divergence. Beam divergence causes significant wall losses inside the channel (~20% of the input power[3]) and a large plume angle (90°) at the exhaust.[4] Dif-

ferent mechanisms could potentially be responsible for this beam divergence.[5–7] For example, because of the high electron temperature (10–20 eV), equipotentials can deviate from the concave magnetic-field surfaces, producing a defocusing electric field in the channel.[5] On the other hand, the presence of curved outward magnetic-field surfaces at the exit of the channel, as well as a fringing magnetic field outside the thruster, can also lead to defocusing of the beam.[6] In addition, the nonuniform distribution of the ion production in the accelerating region can lead to a spread of ion energy distribution, with slower ions affected more strongly by the defocusing electric fields.[7]

In existing Hall thrusters, the electric-field distribution is controlled mainly by the magnetic-field profile along the thruster channel, where $\partial B_r/\partial z > 0$.[1] However, this control by the axial gradient is limited by the practical design and magnetic properties of the magnetic circuit.[2] A Hall thruster with segmented emissive electrodes along the thruster channel can enable further control of the electric-field distribution leading, possibly, to certain advantages over conventional designs.[8,9] Dielectric insulators separate the electrodes, with segments held at different potentials through separate power supplies. Electrons, entering the channel, flow through the electrodes. The radial magnetic field provides magnetic insulation so that very abrupt potential drops, and a very localized acceleration region, can be established in the thruster channel. The localization can be in a region of concave magnetic field for maximum focusing, resulting in less plume divergence.

Flexibly designed laboratory prototype segmented electrode Hall thrusters were built and deployed in the Princeton Plasma Physics Laboratory (PPPL). The segmented electrodes are annular rings, placed either inside the outer ceramic vessel wall or over the inner vessel wall. This is in order to prevent breakdowns between biased segmented electrodes and their shortening by sputtering products during the thruster start and operation. The same magnetic-field lines cross both the conductive surface of an electrode, for example, at the inner wall, and a dielectric surface at the opposite outer wall. It turns out that such an introduction of segmented electrodes has a telling effect on the thruster op-

FIG. 1. Schematic drawing of the Hall thruster.

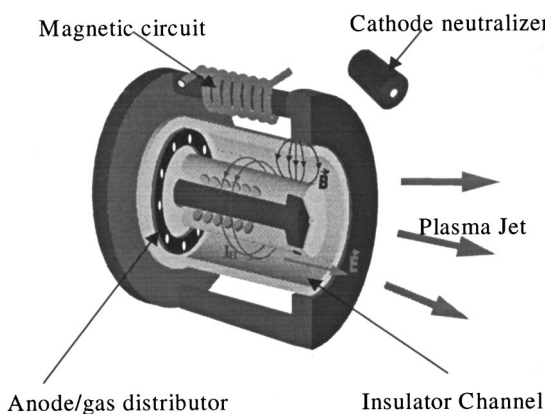
FIG. 2. PPPL model Hall thruster.

eration in ways not anticipated by any simple theory. Not only is their precise placement along the channel significant, but so is their precise shape and emissivity. Moreover, even low emissivity segments held at floating potential can affect thruster operation significantly.[9]

In the present work, we describe results of comprehensive experiments with a low emissivity segmented electrode, which was placed at three different locations at the thruster exit where the magnetic-field lines are curved outward. In such configurations, the thruster is somewhat like a combination of the anode-layer thruster with metal walls[2] and the Hall (so-called magnetic-layer) thruster with dielectric walls. In addition to propulsion applications, there is academic interest in the fundamental physics of the segmented Hall thruster acceleration regime, when the magnetic-field lines connect channel walls made from two different materials with different electrical and secondary emission properties.

II. EXPERIMENTAL SETUP

The vacuum system consists of a 28 m^3 stainless-steel vacuum vessel of a diameter 2.29 m and length 8.38 m equipped with a 35 in. diffusion pump and mechanical vacuum roots pumping system. At a xenon gas flow rate of about 23 sccm, the measured background pressure was about 24 μTorr, corresponding to a pumping speed somewhat larger than 12 000 1/s. To prevent contamination of the thruster and diagnostics due to backstreaming during warm up and cooling of the diffusion pump, this pump is connected to the vessel through a 35 in. right-angle valve. In addition, the thruster and most of the diagnostics are located at the end of the large vacuum vessel, opposite to the right angle flange, which also reduces backstreaming contamination.

Two commercial (Tylan) gas flow controllers FC-260 (0–50 and 0–10 sccm) were used in order to control and measure a xenon gas flow to the anode and cathode of the thruster. In addition to the Millipore LR-250 readout and control box, a pressure gauge was used to verify calibration, stability, and repeatability of the flow meters in the laboratory environment. A set of commercial voltage- and current-regulated power supplies was used in order to support ignition and operation of the thruster, as well as operation of probe diagnostics. The main discharge was supported by a 1
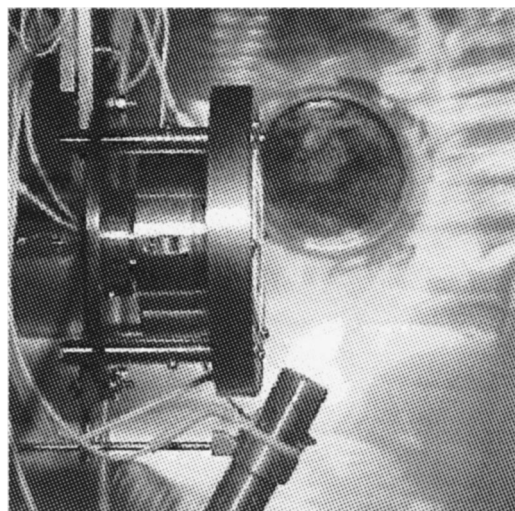
kV, 10 A switching power supply. Separate voltage- and current-regulated supplies were used for biasing of the segmented electrode and electromagnetic coils, respectively.

The 1 kW laboratory Hall thruster (see Fig. 2) is designed modularly to facilitate studies of the thruster operation under different configurations, with and without segmented electrodes. The outer diameter of the channel, which is the characteristic channel dimension, is 90 mm. The magnetic-field distribution in the thruster channel was numerically simulated by using a commercial electromagnetic software package (see Fig. 3) and measured by a Gaussmeter. A typical magnetic-field profile (at a coil current of 2 A) along the thruster axis near the median of the thruster channel is shown in Fig. 4. Here, the radial magnetic field is normalized to its maximum value, which is near the thruster exit.

The segmented electrode, which is referred to below as the negative side, or NS, electrode, is placed along the channel axis on the low potential side at the inner wall. In the present set of experiments, the electrode has about 0.1 mm thickness of LaB$_6$, which was plated in a rhenium mesh to produce a strong structure for the emissive layer. This mesh
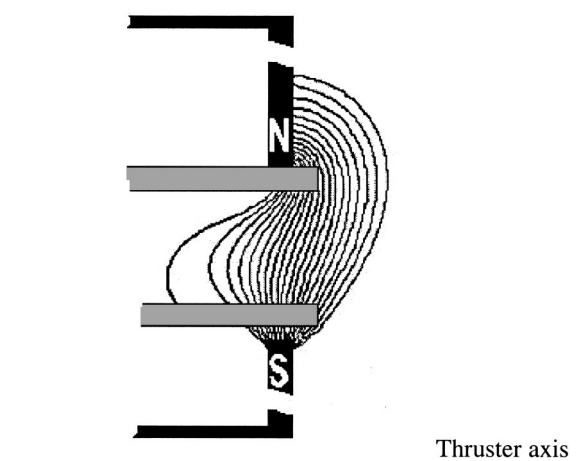

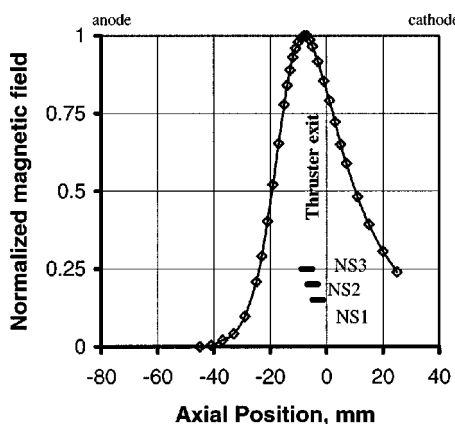FIG. 3. Simulated magnetic field.

FIG. 4. Normalized measured profile of the radial component of the magnetic field along the thruster axis near the channel median at electromagnet coils current of 2 A. NS1, NS2, NS3, are locations of inner-segmented electrodes along the thruster axis.

FIG. 6. Thrust stand and probe setup.

was mounted on a molybdenum substrate ring of 3 mm for each electrode. The length of the NS electrodes was 4 mm. Figure 5 shows this segmented electrode attached to the inner wall of the thruster channel. The voltage potential of the segmented electrode can be floating or biased from a separate power supply or from the main discharge power supply.

The thruster is suspended on an arm of a high-resolution (0.5 mN) pendulum-type thrust stand.[9] Thruster calibration measurements, which were performed throughout the described experiments, exhibited reproducibility better than 1%. Although the smallest difference between calibrating weights, which was reliably detected, was equivalent to a thrust of 0.2 mN, the thrust resolution was taken to be equal to the smallest directly measured calibrating weight,[10] which was equivalent to a thrust of 0.5 mN. The total ion current of the emerging plasma jet and plume parameters (mean cosine angle and plume angle for 90% of the flux) were measured with a flat electrostatic Langmuir probe. The probe, which is a circular disk of about 2 cm diam made from a low sputtering material, was mounted on a positioning mechanism. This mechanism enables the probe to move on a circle with the
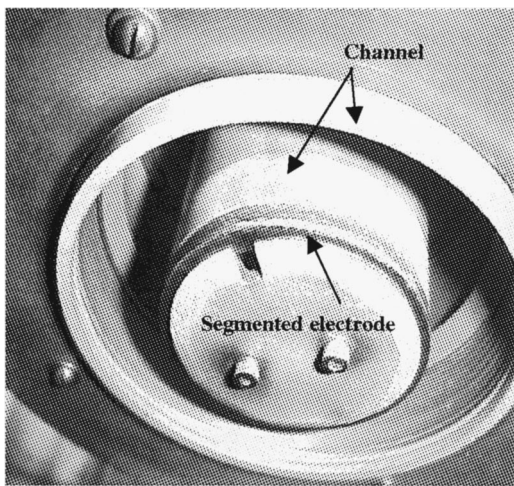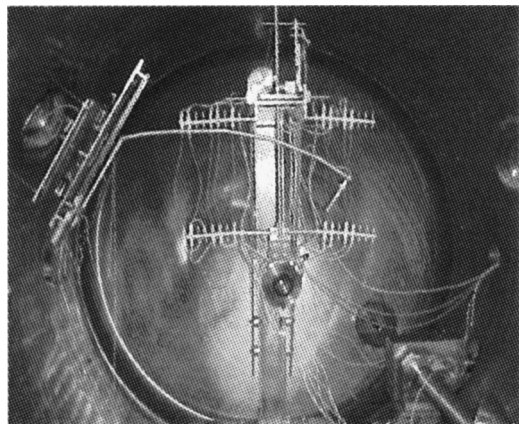
center on the thruster axis, while the radius of the circle can be varied from 33 to about 80 cm. The voltage drop due to the probe current was measured on 100 Ω low inductance shunt. The probe position was measured by a rotating potentiometer. Control of the probe motion and probe measurements were performed by using a data acquisition system which includes an A-T-E series board of National Instruments and LABVIEW software. Figure 6 shows the thruster suspended on the thrust stand and the probe setup.

PC-based digital scopes and spectrum analyzers (DAQ 5102) were used to monitor and characterize discharge oscillations. In voltage mode, the discharge current oscillations were measured on a low impedance shunt. The operating temperature of the inner segmented electrode was measured by a thermocouple, which was fixed on a molybdenum substrate. The surface temperature of the LaB_6 was obtained by an infrared imaging camera TH5104, observing the electrode through a ZnSn window. The camera was calibrated using LaB_6 samples heated to 600 °C.

III. EXPERIMENTAL PROCEDURE

The thruster operation was investigated in eight configurations, including without segmented electrodes (referred to as WS). The segmented configurations are as follows: with one negatively biased or floating segment positioned at the edge of the inner magnetic pole (NS1), with the segment (negative biased or floating) shifted at 2 mm (NS2) and 4 mm (NS3) upstream of the thruster channel relative to the edge of the inner magnetic pole. Figure 4 shows these positions of the segmented electrodes relative to the magnetic-field profile. To evaluate the effect of the segmented electrode, a set of experiments was carried out with a ceramic extension (CE) of the same size as the NS electrode and placed at the same position as the segmented electrode in the NS1 case.

For each configuration, measurements were performed for anode xenon gas flow rates of 1.7, 2, and 2.5 mg/s. In addition, operating regimes with 3 mg/s of the anode flow rate were also investigated as long as breakdown or unstable operation could be avoided. Unstable operation in the high gas flow rate regime can be caused by deposition of the NS electrode material on the outer channel wall. The reproduc-

FIG. 5. Negative side (NS) segmented electrode attached to the inner wall of the ceramic channel.

ibility of these operating regimes was verified by repeating at the beginning, at the middle, and at the end of each thruster run, almost each operating point with segmented electrodes. The discharge current and thrust indicated changes no larger than the measurement error in most of the stable operating points.

The thruster efficiency, $\eta = T^2/mP_e$,[11] was deduced from the thrust T, mass flow m, and input power P_e measurements. The mass flow rate through the cathode, 0.3 mg/s, is not included in the efficiency definition. The relative error in thrust and performance is given in Ref. 10. For example, in the measured operating regimes of the thruster, the relative thrust error was taken equal to the ratio of the thrust resolution to the thrust magnitude, while the relative efficiency error was no more than $\pm5\%$ of the measured value.

Using an electrostatic probe placed at a distance of 33 cm from the thruster exit, the total ion current and plume angle for 90% of the total ion flux I_i from the thruster were measured. Assuming single ionization of xenon propellant, the propellant utilization I_i/I_m was estimated, where $I_m = eM_i/m$, e, and M_i are the equivalent mass flow current, electron charge, and ion mass, respectively.[11] For certain operating points, plume measurements were repeated several times at certain angles. The repeatability of the full plume angle was about $\pm4°$.

IV. EXPERIMENTAL RESULTS

During operation with the NS electrode, the maximum electrode temperature was measured by a thermocouple when the thruster was at steady state. In the case of NS1, the surface temperature of LaB_6 was also measured with an infrared camera. The maximum temperature from the thermocouple (about $1040\,°C$) was obtained with the electrode at the NS1 position, with operation at a discharge voltage of 300 V and mass flow rate of 3 mg/s. At this operating point, infrared measurements showed the maximum of $1100\,°C$ at the LaB_6 surface. The temperature dropped when the input power was reduced. Also, at the same operating point, the temperature measured by the thermocouple was about 900 and $700\,°C$ for NS2 and NS3 electrode cases, respectively. The reduction with the power is most probably due to a decrease in the energy of ions hitting the wall. An alternative explanation might be that by shifting the electrode from NS1 to NS3 along the thruster channel, the ion flux to the segmented electrode decreases, which would also lead to a reduction in the electrode temperature.

Figure 7 shows illustrative curves of voltage versus current characteristics ($V-I$) measured at two anode mass flow rates of 1.7 and 2.5 mg/s for seven different configurations of the thruster, WS, NS1, NS2, and NS3. Here, in each segmented electrode case, the $V-I$ curve was measured for the NS electrode under floating potential and cathode bias. Each point on these curves was obtained at the minimum of the discharge current versus the magnetic field.[12] In addition, Fig. 8 shows the propellant utilization versus the discharge voltage for the same configuration at 1.7 and 2 mg/s. Figures 9 and 10 compare $V-I$ characteristics and propellant utiliza-
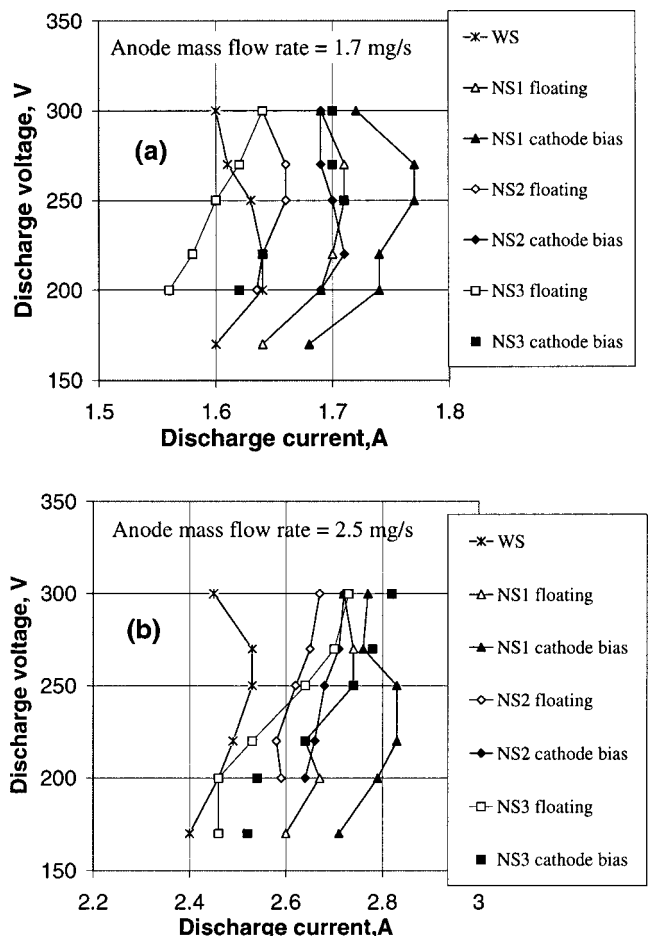

FIG. 7. $V-I$ characteristics of the thruster for the seven thruster configurations: WS; and NS1, NS2, and NS3 (floating and under cathode bias) at 1.7 mg/s (a) and 2.5 mg/s (b).

tion the thruster without segmented, with the CE channel, and NS1.

As can be seen from $V-I$ curves, at both mass flow rates and at a given discharge voltage, the discharge current measured without segmented electrodes was generally less than that with segmented electrodes for a variety of different configurations and operating regimes. As we move the NS electrode upstream in the channel, the $V-I$ characteristics shift towards smaller currents at given discharge voltage and mass flow rate. Also, the current tends to increase at all three locations when the cathode bias was applied to the segmented electrode. However, the discharge current measured at 1.7 mg/s for the NS3 under floating potential is less than that measured for the WS configuration. Moreover, at 2.5 mg/s, as the gas flow rate is increased, the discharge current, which at the thruster exit is mainly carried by ions, increases, too.

At most operating points, the propellant utilization is higher with the ''without segment'' configuration than with any negative side segmented cases for mass flow rates 1.7 and 2.0 mg/s (see Fig. 8). Similar results were measured with anode mass flow rates of 2.5 and 3 mg/s. Consistent with lower propellant utilization and larger discharge current, the ratio of the ion current to the discharge current is also larger for the ''without segment'' case.
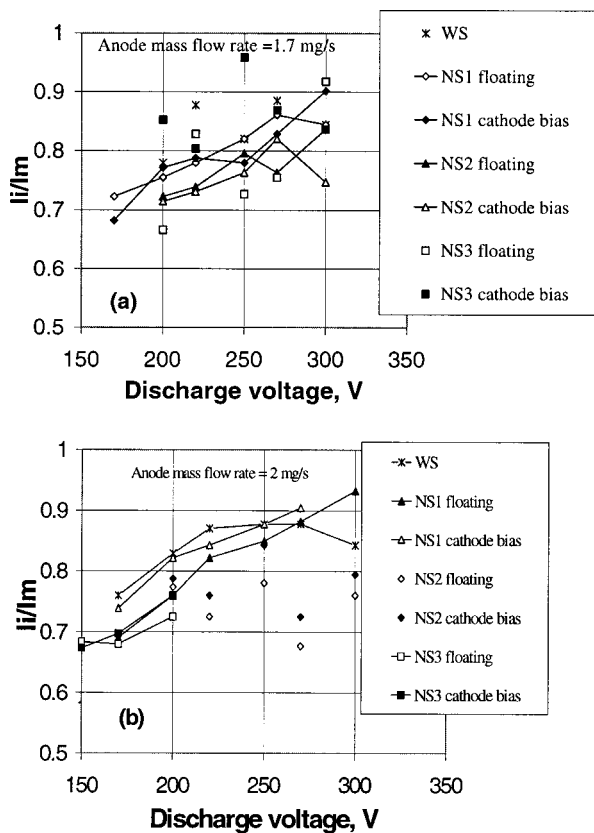
FIG. 8. Propellant utilization vs the discharge voltage measured for the seven thruster configurations WS, NS1, NS2, and NS3 (floating and under cathode bias) at 1.7 mg/s (a) and 2 mg/s (b).

FIG. 10. Propellant utilization vs discharge voltage measured for four thruster configurations WS, NS1 (floating and under cathode bias), and CE at 1.7 mg/s.

2.5 mg/s, and different configurations of the thruster. Note that at the small mass flow rate of 1.7 mg/s, a smaller plume half angle (about 10°) occurred under the NS configuration, in particular, under the biased NS2 case. When the mass flow rate is increased, the differences become comparable to the error in the reproducibility of the probe measurements. However, there is an indication of generally smaller plumes for the WS case for mass flow rates higher than 2.5 mg/s.

V. DISCUSSION AND SUMMARY

An explanation of the behavior of the thruster with the NS electrode cases might be along the following lines: According to Refs. 2 and 13, under typical Hall thruster and anode-layer thruster conditions, say $T_e \sim 10$–50 eV, $V_i \sim 10^3$ eV, the secondary emission δ from the metal wall of the thruster channel is negligible. Hence, no ''cooling'' of electrons takes place in the channel with metal walls. Thus, the electrons gain kinetic energy, which is randomized by collisions, on a shorter distance than with ceramic walls. This may increase the gradient of electron pressure, thus affecting both the voltage potential distribution and the radial plasma sheath. For example, in Ref. 14, a reduction of the acceleration and ionization region and an increase of the discharge current were experimentally observed. In that case, the sputtering of a metal target placed outside the thruster caused metalization of ceramic walls. An increase in the discharge current as compared to the ''clean'' channel walls is attributed to discharge current oscillations. Note that anode-layer thrusters have a shorter accelerating layer, and the magnetic field is twice as strong as in Hall thrusters with ceramic walls.[2]

The increased values of the discharge current at given mass flow rates, which were observed in the experiments with floating segmented electrodes (See Fig. 7), may result from such a metalization of the outer wall by sputtering of the negative side segmented electrode placed on the inner wall. In order to prevent this contamination, a set of small grooves was inserted into the outer wall of the channel, which gave stable long duration operation of the thruster with reproducible measurements. Nevertheless, trace

When the ceramic extension was placed at the position NS1, the discharge current increased even more than it was in the case of the NS1 electrode at that position for the same discharge voltage and mass flow rate. This increase, which was typical at all mass flow rates, is illustrated in Fig. 9. However, the ion propellant utilization (Fig. 10) almost did not change and, therefore, the ratio of the ion current to the discharge current is less compared to what it is for the WS configuration of the thruster.

Figure 11 shows the half-plume angle versus the discharge voltage measured at three mass flow rates, 1.7, 2, and
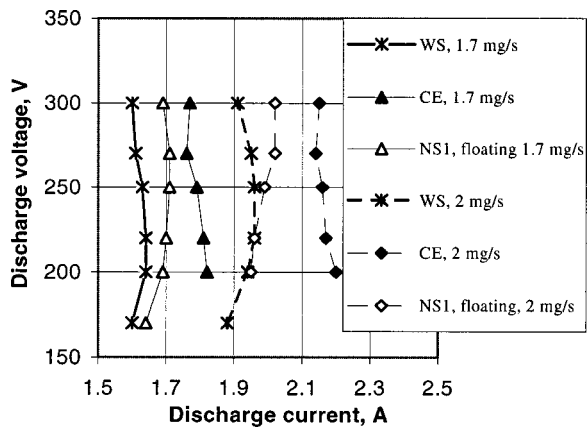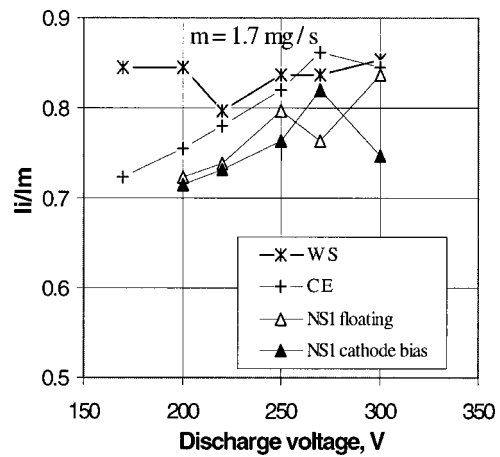

FIG. 9. V–I characteristics for three thruster configurations WS, NS1 (floating and under cathode bias), and CE, at 1.7 and 2 mg/s.
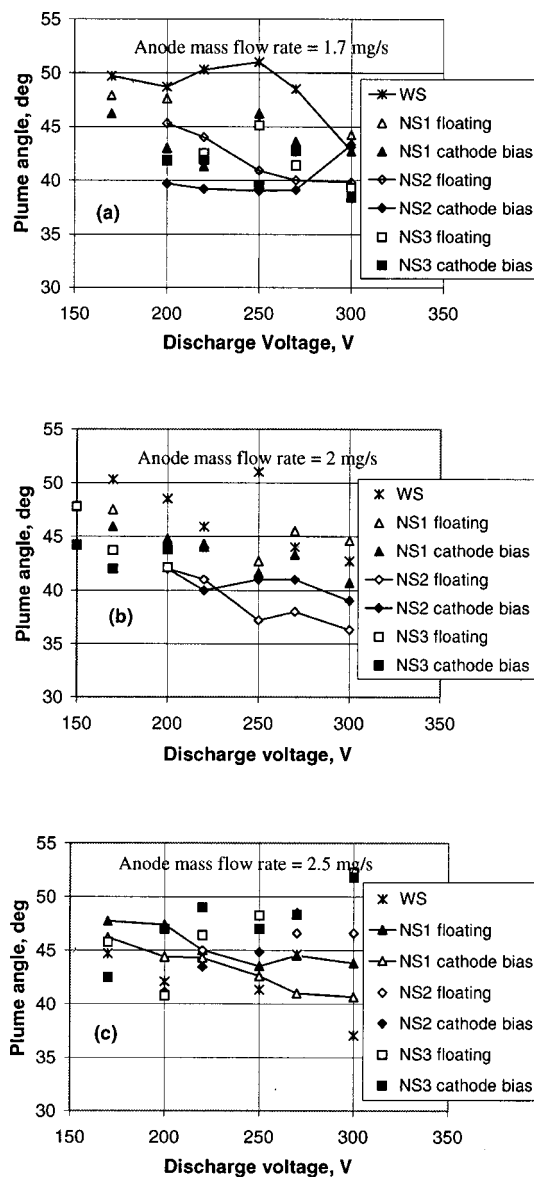
FIG. 11. Half-plume angle estimated for 90% of the measured ion flux from the thruster of different configurations (WS, NS1, NS2, and NS3, floating, biased) at three different mass flow rates.
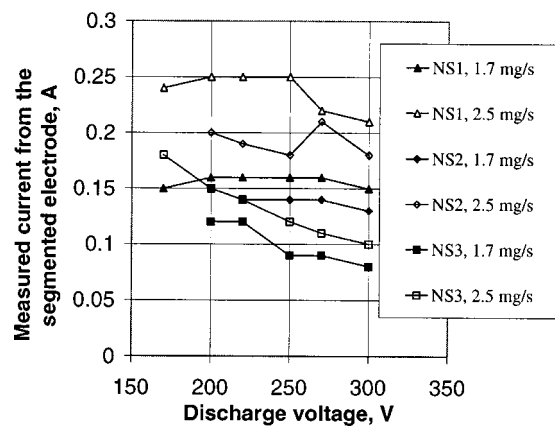

FIG. 12. Current to the segmented electrode, measured for three segmented electrode configurations, NS1, NS2, and NS3 (under cathode bias) measured at two mass flow rates 1.7 and 2.5 mg/s.

amounts of the electrode material were detected by x-ray spectrometer in postrun inspection of the thruster channel walls. After a long run of the thruster, the presence of a conductive layer could be observed even with an Ohm meter. This layer is particularly large in the NS1 electrode case, much smaller in the NS2, but not in the NS3.

The observed differences in the channel metalization for the NS thruster cases is apparently due to more energetic ions arriving at the edge of thruster channel,[7,11] which in the present set of experiments corresponds to the location of NS1. Hence, the stronger metalization of the outer ceramic walls takes place for electrode placement NS1. However, in contrast to Ref. 14, the amplitude of the discharge current oscillations measured in all NS electrode cases were not larger, but smaller than in the WS case. Therefore, a possible cause of the increased discharge current in the floating NS cases is a smaller magnetic insulation of the acceleration region with a larger electric field as compared to the WS case. Indeed, although ''optimal'' values of the coils' current (magnetic field) in the NS cases were larger by roughly 10%–30% than in the WS case, it was not possible to operate with the magnetic field double the amplitude of the optimal value typical for an anode-layer thruster. This limitation was due to the overheating of the electromagnetic coils and saturation of the magnetic core at large gas flow rates. An indication of the reduced magnetic insulation is that the larger fraction of the axial electron current for the NS cases can be derived from results of $V-I$ characteristics and propellant utilization versus the discharge voltage (Figs. 7 and 8, respectively).

When the segmented electrode is biased under the cathode potential it can collect ions from the plasma, thus contributing to the discharge current. An additional electric circuit path runs parallel to the main circuit between the anode and cathode neutralizer. This is likely why the discharge current with the biased segmented electrodes is larger than in the corresponding floating cases.

Figure 12 shows the current to NS segmented electrode at the cathode bias at three different positions: NS1, NS2, and NS3 and at two mass flow rates, 1.7 and 2.5 mg/s. As can be seen, when the segmented electrode is moved inside the thruster channel, the current tends to decrease. At a given mass flow rate and electrode position, the measured current to segmented electrode tends also to decrease as the discharge voltage is increased. Note that from the above explanations this current is likely an ion current. Note that the reduction of the current to the segmented electrode, as it is moved upstream to the maximum magnetic field, does not necessarily mean a reduction of the effect of this electrode on the acceleration and ionization region. Figure 13 shows that the floating potential of the segmented electrode does not change with the discharge voltage in the NS1 configuration, but rather drops with the NS3 case when the discharge voltage is above 250 V at 1.7 mg/s and above 220 at 2.5 mg/s. In the NS2 case, changes in the floating potential with the discharge voltage are also insignificant at the small mass flow rate. On the other hand, at 2.5 mg/s the behavior of the potential versus the discharge voltage is closer to the NS3
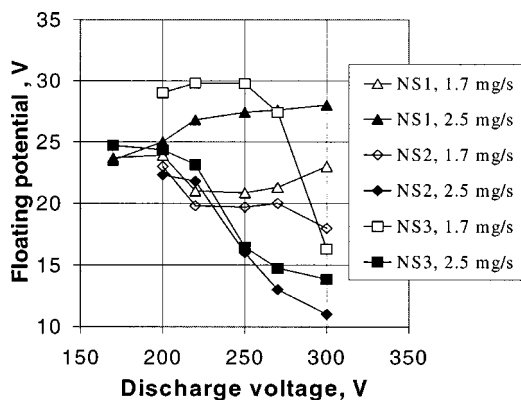
FIG. 13. Floating potential measured between the cathode and segmented electrode for three segmented electrode configurations NS1, NS2, and NS3 at two mass flow rates 1.7 and 2.5 mg/s.

FIG. 14. Thrust vs discharge voltage measured at two mass flow rates, 1.7 mg/s for WS, NS1, NS2, and NS3 (a) and 2.5 mg/s for WS, NS2, and NS3 (b).

case at the same mass flow rate. The difference in the behavior of the floating potential may be also attributed to changes in the length or motion of the acceleration region as the discharge voltage is varied. The behavior of the potential with gas flow rate at a given discharge voltage might also be attributed to changes in the acceleration region length as the electron temperature and atomic density increase with the mass flow and more ionization collisions take place closer to the thruster exit.

In the CE case (see Fig. 9), the increase of the discharge current as compared to the WS at a given discharge voltage can also be, in principle, attributed to the sputtering of the ceramic extension with subsequent coating of the channel walls by a boron-nitride dust. In Ref. 14, similar behavior of the discharge current was observed with quartz dust on a boron-nitride channel. However, since for silicon $\delta \sim 1$ at 300 eV,[14] quartz dust produces an increase in the electron temperature similar to that produced by metal walls. On the other hand, in our experiments, the dust and channel were of the same ceramic material and, therefore, had the same secondary emission coefficients. As a possible explanation, in addition to electron wall collisions, wall recombination losses at the ceramic extension may result in an increase of the atomic density at the thruster exit. That may be an additional source of degradation of the magnetic insulation in the acceleration region relevant for the CE case and, at least, for the NS3 segmented electrode.

In principle, depending on their location, either relative to each other or to the magnetic field and the electron temperature, two channel wall segmented electrodes made from different materials should be able to affect defocusing or focusing of the ion beam, and as a result the propellant utilization and plume. For example, it was suggested in Ref. 15 that due to a larger potential difference between the plasma and the floating metal wall, the ion flux to the wall will increase in the most of the acceleration and ionization region, leading to an increase of ion losses. In addition, Ref. 14 attributed the measured reduction of the ion current with metalized channel walls to a degradation of the ionization conditions and an increase of ion energy distribution in a shorted ionization and acceleration region. Thus, it might be expected that the plume angle should also be larger in the
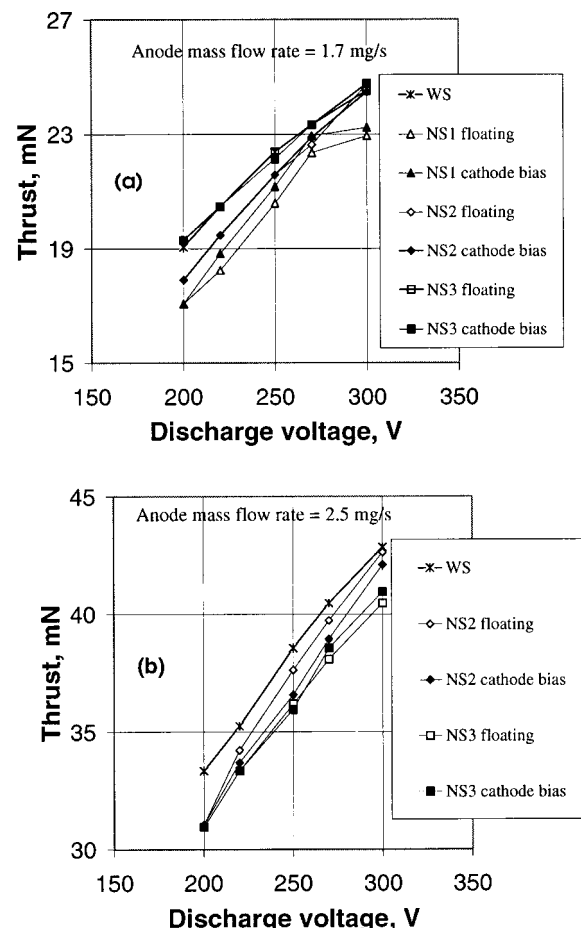
channel with metal walls compared to with ceramic walls. Both of these explanations may pertain also to the propellant utilization with the segmented electrode thruster (see Fig. 8).

Most likely, different mechanisms account for the reduction of the plume angle with segmented electrodes and only slight degradation of the propellant utilization within the accuracy of the probe measurements at some discharge voltage (see Fig. 8) and small mass flow. These improvements over the WS case may be attributed, for example, to different secondary emission coefficients of the ceramic and metal walls along the same magnetic-field lines, resulting in different sheath and presheath potential drops. The thickness of these drops varies with the operating conditions and inclination of the magnetic-field lines to the electrode surface.[16] Another possible explanation is that at small mass flow rates the ionization mean-free path increases, leading to less efficient ionization and larger ion losses in the conventional thruster configuration.[17] The metal walls may permit an increase in the electron temperature and, as a result, may provide for ionization in a shorter region with less losses. It is also possible that since the segmented electrode is biased under the cathode potential it may also collect slow ions, which contribute to the plume at large angles.[7]

Figures 14 and 15 show thrust and thruster efficiency versus the discharge voltage for mass flow rates at 1.7 and
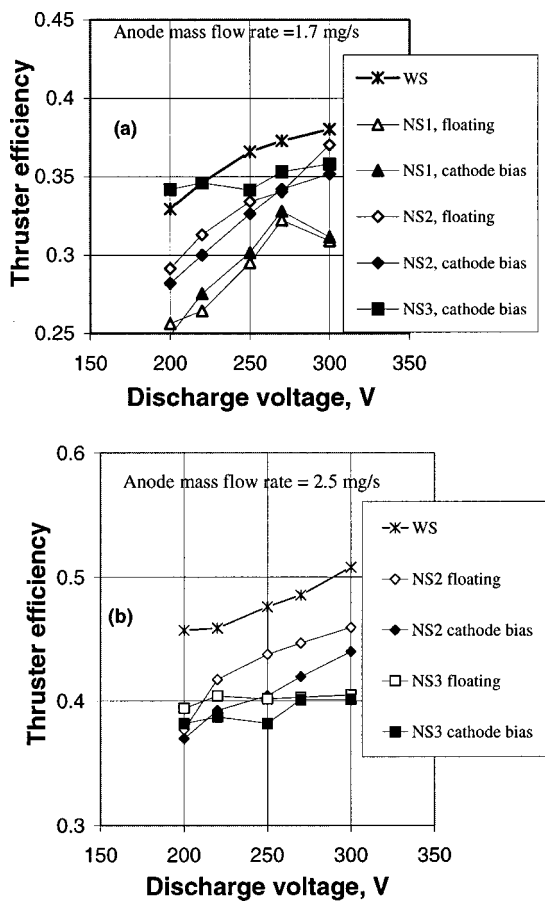
FIG. 15. Thruster efficiency vs discharge voltage measured for WS and NS1, NS2, and NS3 floating and biased configurations at two mass flow rates: 1.7 mg/s (a) and 2.5 mg/s (b).

2.5 mg/s, for each of the seven configurations with the NS segmented electrode and without the segmented electrode. Note that the thrust and efficiency are somewhat better with the nonsegmented configuration at most of the operating points, voltage, and mass flow rates, and different configurations, as might be expected given the measurement of propellant utilization versus the discharge voltage (Fig. 8) and the $V-I$ characteristics (Fig. 7). Note, too, that this rather small general decrease in thrust and efficiency for segmented

electrode operation comes with the more significant general improvement in plume divergence.

In summary, while the measurements here exhibit the very promising decreased plume divergence, and some working hypotheses can be put forth, a better understanding of the effect of the segmented electrode on integral characteristics of the Hall thruster and its plume will require local measurements of the plasma parameters inside the thruster and a more detailed theoretical analysis.

ACKNOWLEDGMENTS

[1] A. I. Morozov, Yu. V. Esipchuk, A. M. Kapulkin, V. A. Neverovskii, and V. A. Smirnov, Sov. Phys. Tech. Phys. **17**, 482 (1972).
[2] V. V. Zhurin, H. R. Kaufman, and R. S. Robinson, Plasma Sources Sci. Technol. **8**, 1 (1999).
[3] M. Martinez-Sanchez and J. E. Pollard, J. Propul. Power **5**, 688 (1998).
[4] S. N. Askhabov *et al.*, Sov. J. Plasma Phys. **7**, 125 (1981).
[5] A. I. Morozov, A. I. Bugrova, V. A. Ermolenko, and L. A. Lein, Sov. Phys. Tech. Phys. **33**, 185 (1988).
[6] M. Keidar and I. D. Boyd, J. Appl. Phys. **86**, 1 (1999).
[7] L. B. King and A. D. Gallimore, American Institute of Aeronautics and Astronautics Paper No. 96-2712, Lake Buena Vista, FL, 1996.
[8] A. Fruchtmann and N. J. Fisch, American Institute of Aeronautic and Astronautics Paper No. 98-3500, Cleveland, OH, 1998.
[9] N. J. Fisch, Y. Raitses, A. A. Litvak, and L. A. Dorf, American Institute of Aeronautics and Astronautics Paper No. 99-2572, Los Angeles, CA, 1999.
[10] J. R. Brophy, Jet Propulsion Laboratory No. JPL-92-4, 1992.
[11] V. Kim, J. Propul. Power **14**, 736 (1998).
[12] Y. Raitses and J. Ashkenazy, Proceedings of the XVII International Symposium on Discharges and Electrical Insulation in Vacuum, Berkeley, CA, 1996.
[13] A. I. Morozov, Sov. Phys. Tech. Phys. **32**, 901 (1987).
[14] A. I. Bugrova, A. V. Desyatkov, A. I. Morozov, and V. K. Kharchevnikov, Plasma Phys. Rep. **22**, 302 (1996).
[15] B. B. Egorov, V. Kim, A. A. Semenov, and I. I. Shkabran, in *Ion Injectors and Plasma Accelerators*, edited by A. I. Morozov and N. N. Semashko (Energoatomizdat, Moscow, 1990) (in Russian).
[16] I. I. Beilis and M. Keidar, Phys. Plasmas **5**, 1543 (1998).
[17] Y. Raitses, J. Ashkenazy, and M. Guelman, J. Propul. Power **14**, 247 (1998).